

Concerted Ion Migration and Diffusion-Induced Degradation in Lead-Free Ag_3BiI_6 Rudorffite Solar Cells under Ambient Conditions

Ashish Kulkarni,* Feray Ünlü, Namrata Pant, Jagjit Kaur, Christoph Bohr, Ajay Kumar Jena, Senol Öz, Masatoshi Yanagida, Yasuhiro Shirai, Masashi Ikegami, Kenjiro Miyano, Yasuhiro Tachibana, Sudip Chakraborty, Sanjay Mathur,* and Tsutomu Miyasaka*

Dedicated to Anil Madhavrao Deshpande (Kaka Saheb) and others who lost their life due to COVID-19.

Silver bismuth iodide (SBI) materials have recently gained attention as nontoxic alternatives to lead perovskites. Although most of the studies have been focusing on photovoltaic performance, the inherent ionic nature of SBI materials, their diffusive behavior, and influence on material/device stability is underexplored. Herein, AgBiI_2 , Ag_2BiI_5 , and Ag_3BiI_6 thin films are developed in controlled ambient humidity conditions with a decent efficiency up to 2.32%. While exploring the device stability, it is found that Ag_3BiI_6 exhibits a unique ion-migration behavior where Ag^+ , Bi^{3+} , and I^- ions migrate and diffuse through the dopant-free hole transport layer (HTL) leading to degradation. Interestingly, this ion-migration behavior is relatively fast for the case of antisolvent-processed Ag_3BiI_6 thin-film-based devices contrasting the case of without antisolvent and is not observed for other SBI material-based devices. Theoretical calculations suggest that low decomposition enthalpy favors the decomposition of Ag_3BiI_6 to AgI and BiI_3 causing migration of ions to the electrode which is protected by using a thick HTL. The new mechanism reported herein underlines the importance of SBI material composition and fundamental mechanism understanding on the stability of Ag_3BiI_6 material for better solar cell design and also in extending the applications of unique ion-migration behavior in various optoelectronics.

1. Introduction

Organic–inorganic hybrid lead halide perovskite solar cells have witnessed a rapid rise in power conversion efficiency (PCE) from 3.8% to certified 25.5%.^[1–3] Despite such advantages, perovskite degrades after exposure to moisture, heat, light, and oxygen.^[4] In addition to this, intrinsic factors such as ion migration,^[5] defects,^[6] material instability,^[7] and nature of adjacent charge transport layers^[8] also affect the stability of the material. As a result, water-soluble ionic lead (Pb^{2+}) cation is released as an inherently toxic byproduct.^[9] Development of lead-free perovskite and perovskite-inspired semiconducting materials with improved stability and efficiency is vital and is at the forefront of the research focus. Replacement of Pb^{2+} with tin (Sn^{2+}) was demonstrated first due to similar structural and electronic configurations. However,

Dr. A. Kulkarni, Dr. A. K. Jena, Dr. S. Öz, Prof. M. Ikegami, Prof. T. Miyasaka
Graduate School of Engineering
Toin University of Yokohama
1614, Kurogane Cho, Aoba, Yokohama, Kanagawa 225-8503, Japan
E-mail: a.kulkarni@fz-juelich.de; miyasaka@toin.ac.jp


Dr. A. Kulkarni
IEKS-Photovoltaics
Forschungszentrum Jülich
52425 Jülich, Germany

F. Ünlü, C. Bohr, Prof. S. Mathur
Department of Chemistry
Institute of Inorganic Chemistry
University of Cologne
Greinstrasse 6, 50939 Cologne, Germany
E-mail: sanjay.mathur@uni-koeln.de

Dr. N. Pant, Prof. M. Yanagida
Integrated Graduate School of Medicine
Engineering and Agricultural Sciences
University of Yamanashi
4 Chome-4-37 Takeda, Kofu 400-8510, Japan

J. Kaur, Dr. S. Chakraborty
Materials Theory for Energy Scavenging (MATES) Lab
Discipline of Physics
Indian Institute of Technology
Indore 453552, India

J. Kaur, Dr. S. Chakraborty
Materials Theory for Energy Scavenging (MATES) Lab
Harish-Chandra Research Institute (HRI) Allahabad
Chhatnag Road, Jhansi, Allahabad 211019, India

 The ORCID identification number(s) for the author(s) of this article can be found under <https://doi.org/10.1002/solr.202100077>.

DOI: 10.1002/solr.202100077

Dr. S. Öz
Saule Technologies, and Saule Research Institute
Dunska 11, 54-427 Wrocław, Poland

rapid oxidation of Sn^{2+} to Sn^{4+} under ambient atmosphere makes tin-based perovskite even more unstable than their lead counterparts.^[2,9,10] Due to its isoelectronic ($6s^2$) nature, efforts have been made to replace Pb^{2+} with bismuth (Bi^{3+}).^[11] The assimilation of protonated cations such as methylammonium (MA^+) or cesium (Cs^+) into Bi-I octahedra forms Bi-based ternary halides ($\text{A}_3\text{Bi}_2\text{I}_9$; $\text{A} = \text{MA}^+, \text{Cs}^+$). These materials exhibit high absorption coefficients similar to lead perovskites and stability under ambient humidity atmosphere. Nevertheless, the photovoltaic device performance of $\text{A}_3\text{Bi}_2\text{I}_9$ absorber materials remained low mainly due to wide indirect bandgap (E_g), high exciton binding energy, low electronic dimensionality induced anisotropic charge transport,^[12,13] background carrier densities, and poor charge carrier mobility.^[14,15]

Replacement of A-site cations (MA^+, Cs^+) with transition metals such as silver (Ag^+) or copper (Cu^+) results in the formation of a 3D edge-sharing octahedral network along with the reduction in optical bandgap (from 2.3 eV for $\text{A}_3\text{Bi}_2\text{I}_9$ to <1.8 eV). Although these materials have been studied for several decades because of interesting optoelectronic properties and high ionic conductivity, their photovoltaic device performance has been realized lately. Initially, Sargent and coworkers have used AgBi_2I_7 as an absorber material and reported a PCE of 1.22%.^[16] Recently, we tuned the crystallization of AgBi_2I_7 by using a weak solvent-intermediate adduct and reported PCE of 2.3% with high stability and reproducibility.^[17] The photovoltaic device with hexagonal Ag_2BiI_5 absorber, as demonstrated by Johansson and coworkers, showed PCE of 2.1% in mesoscopic device architecture.^[18] Turkevych et al. used Ag_3BiI_6 light absorber in mesoscopic architecture and the device with poly[bis(4-phenyl)(2,4,6-trimethylphenyl)amine (PTAA) hole transport layer (HTL) showed PCE of 4.3%.^[19] Recently, Pai et al. used argon (Ar) gas quenching during the spin-coating step to obtain Ag_3BiI_6 film and achieved a PCE of 4.38% and 2.69% with PTAA and poly-3-hexylthiophene-2,5-diyl (P3HT) HTL, respectively.^[20] Dynamic casting with ramp annealing step, as demonstrated by Seo and coworkers, improved the morphology, and the inverted planar Ag_3BiI_6 device with nickel oxide (NiO_x) HTL showed a PCE of 1%.^[21] Although these studies^[19–22] have demonstrated decent initial efficiency and stability over hybrid lead perovskites, the inherent ionic nature of silver bismuth iodide (SBI) materials raises analogous ion migration concerns that effects device long-term stability.

Ion migration in hybrid lead halide perovskite has been rigorously studied and is revealed to be a contributing factor for ferroelectricity,^[23] hysteresis behavior in the device current-voltage characteristic curve,^[24] and device operational stability.^[25] Due to the low activation energy, halide anions and A-site cations in ABX_3 perovskite crystal structure ($\text{A} = \text{MA}^+, \text{Cs}^+$; $\text{B} = \text{Pb}^{2+}$; $\text{X} = \text{I}^-, \text{Cl}^-, \text{Br}^-$) are found to be the migrating species, while the metal (Pb^{2+}) cation tends to be immobile.^[26] On the contrary, to the best of our knowledge, very little is known about the ion migration in SBI materials. Oldag et al. reported the activation energy of Ag^+ cations migration to be 0.4 eV in the Ag_3BiI_6 single crystal which is similar to the activation energy of iodine migration

(0.44 eV) in lead halide perovskites.^[27] However, experimental evidence on the ion migration^[28,29] of Ag_3BiI_6 material and its dependence on the thin-film deposition method remains rare, such as the mobile species, their diffusive behaviors, and their influence on material/device stability. Herein, we report a unique ion-migration behavior of Ag_3BiI_6 solar cells using dopant-free P3HT HTL. Contrasting the predominant role of halide in ion migration in widely studied lead halide perovskites, we found that Ag_3BiI_6 -based devices adopt a unique triple-ion-migration-induced degradation, where Ag^+ , Bi^{3+} , and I^- migration and diffusion occur in the long-term operation of the devices. This migration is also dependent on the thin-film deposition method and on compositions of the SBI material and only occurs in the Ag-rich phase material. From theoretical studies, we observed that the decomposition reaction of Ag_3BiI_6 into silver iodide (AgI) and bismuth iodide (BiI_3) is exothermic and therefore thermodynamically favored, which can be the main reason for the migration of ions. This migration of ions to the gold electrode can be protected by using thick HTL and also by using the suitable SBI composition containing less amount of Ag-rich phase to fabricate solar cells.

2. Results and Discussion

SBI thin films were obtained by dissolving 50 wt% each of AgI and BiI_3 in a stoichiometric ratio in dimethylsulfoxide (DMSO) followed by spin coating the solution on TiO_2 mesoporous layer-coated FTO substrates and annealing at 85 °C for 5 min and at 100 °C for 20 min. For the antisolvent dripping, 1 mL of chlorobenzene (CB) was dropped over the substrate during the spin coating step as shown in Figure S1, Supporting Information, and outlined in the Experimental Section in the Supporting Information. Figure 1a shows the schematic illustration of the device architecture using AgBi_2I_7 , Ag_2BiI_5 , and Ag_3BiI_6 materials. It is important to note that we used a hot-casting method to obtain SBI (AgBi_2I_7 , Ag_2BiI_5 , and Ag_3BiI_6) thin films because the process has been previously reported to improve device performance.^[19] The formation of different SBI materials deposited via the antisolvent method was monitored using X-ray diffraction (XRD) measurements and the results are in agreement with the previous reports.^[16,18,19] Figure S2, Supporting Information, compares the literature diffraction data with the experimental one showing the peak positions and relative intensities. In addition to the XRD signatures of SBI materials, additional peaks were observed in the XRD patterns (marked with * in Figure 1b) assigning to AgI. This indicates the presence of residual or unreacted AgI in the SBI films. The residual AgI peak intensity increases with an increase in the AgI content in the SBI material showing the order of $\text{Ag}_3\text{BiI}_6 > \text{Ag}_2\text{BiI}_5 > \text{AgBi}_2\text{I}_7$, as shown in Figure 1b and Figure S3, Supporting Information. Koedtrud et al. reported that for several compositions of Ag–Bi–I materials in particular Ag_3BiI_6 and Ag_2BiI_5 , the related phases and AgI coexist at room temperature, which we observed in our study.^[30] In the case of

Prof. M. Yanagida, Prof. Y. Shirai, Prof. K. Miyano
Centre for Green Research on Energy and Environmental Materials
National Institute for Materials Science (NIMS)
1-1 Namiki, Tsukuba, Ibaraki 305-0044, Japan

Prof. Y. Tachibana
School of Engineering
RMIT University
Bundoora, VIC 3083, Australia

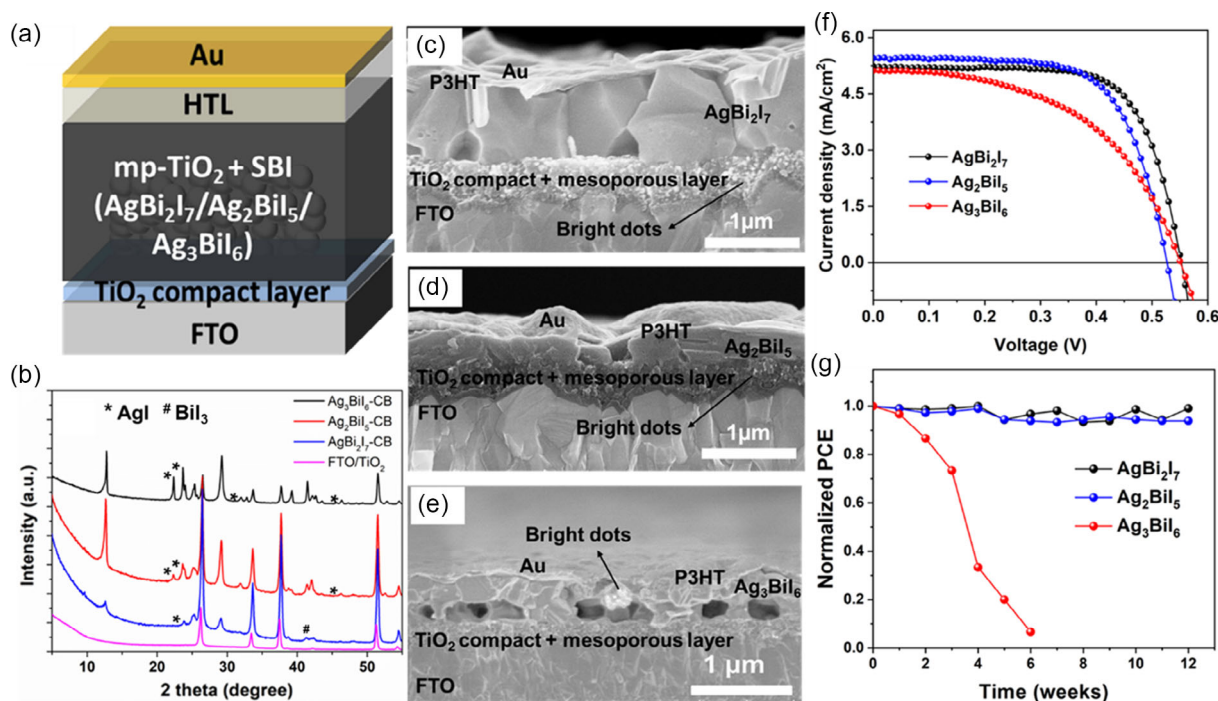


Figure 1. Comparison of SBI material properties and photovoltaic performance a) n-i-p mesostructured device architecture; b) XRD patterns obtained from thin films of Ag₃BiI₆ (black), Ag₂BiI₅ (red), and AgBi₂I₇ (blue) on FTO/TiO₂ substrate (magenta) showing residual AgI in all the SBI materials and residual BiI₃ in AgBi₂I₇; c–e) cross-sectional SEM images of the SBI solar cell devices processed with antisolvent; f) J–V curves of best performing SBI solar cells; and g) stability of the best performing SBI solar cells over several weeks.

the Ag-deficient composition AgBi₂I₇, the obtained XRD pattern is consistent with the previous report by Mashadieva et al.^[31] additionally with a doublet peak at 42°. Previously, we reported that this doublet peak is due to remnant BiI₃ which plays an important role in enhancing the performance and stability of AgBi₂I₇ solar cells.^[17] The difference in the peak intensity of residual AgI in Ag₃BiI₆ compared with previous reports^[19,20,32] might be due to the fabrication of thin film in an ambient atmosphere with controlled humidity and the use of DMSO solvent (see the Experimental Section for more details). Cross-sectional scanning electron microscopy (SEM) micrographs of AgBi₂I₇ (Figure 1c) and Ag₂BiI₅ (Figure 1d) showed uniform interface with adjacent charge transport layers whereas, in the case of Ag₃BiI₆, a large number of voids were observed (Figure 1e) near the TiO₂ interface. Another cross-sectional SEM image of the Ag₃BiI₆ device showing voids over a large area is shown in Figure S4, Supporting Information. Different crystallization process on the surface and at Ag₃BiI₆/TiO₂ interface (as illustrated in Figure S5, Supporting Information, and explained in Explanation E1, Supporting Information) is suspected to be the reason for the formation of voids. In addition to this, bright dots were observed in all the cases, as shown in cross-sectional SEM images (Figure 1c–e), which can be attributed to aggregates of the Ag-rich phase.^[33,34] Previously, Bekenstein et al. also observed the formation of the Ag-rich phase in Cs₂AgBiBr₆ nanocrystals due to the less-standard reduction potential of silver.^[33] Interestingly, in the case of AgBi₂I₇ and Ag₂BiI₅, bright dots were

observed only on the surface of the TiO₂ mesoporous layer whereas in the Ag₃BiI₆ case, they were observed on the surface of Ag₃BiI₆ and Au metal electrode, as shown in Figure 1c–e, respectively. Another cross-sectional SEM image of the Ag₃BiI₆ device showing accumulation of white dots (Ag-rich phase) on the surface of the Au metal electrode is shown in Figure S6, Supporting Information. The presence of voids at the bottom interface (Figure 1e and Figure S4, Supporting Information) and bright dots on the surface of the Ag₃BiI₆ layer and Au metal electrode (Figure 1e and Figure S6, Supporting Information) indicates the more accumulation of AgI (Ag-rich phase) near the Ag₃BiI₆/P3HT/Au interface. Moreover, the presence of voids and nonuniform interfacial connection indicates that the Ag₃BiI₆ device undergoes high internal resistance and/or large recombination and improper interfacial charge transfer and might result in low device efficiency compared with AgBi₂I₇ and Ag₂BiI₅. As expected, the current density (J)–voltage (V) characteristic curves of the best performing photovoltaic device, as shown in Figure 1f, incorporating AgBi₂I₇, Ag₂BiI₅, and Ag₃BiI₆ absorber with P3HT HTL showed PCE of 2.1%, 2.04%, and 1.8%, respectively. The photovoltaic device parameters of best-performing device J–V curves and statistics showing the reproducibility of the device performance are tabulated in Table S1 and Figure S7, Supporting Information, respectively. While exploring the device stability in ambient humidity (RH = 30–50%) atmosphere, it was interesting to observe that AgBi₂I₇ and Ag₂BiI₅ devices showed stable

efficiency for ≈ 12 weeks whereas Ag_3BiI_6 device performance started degrading within 2 weeks, as shown in Figure 1e. This degradation was accompanied by the visual change in the color of the Au metal electrode which turned from yellow to greenish-yellow, as shown in Figure S8, Supporting Information. This was also observed by Crovetto et al., who suspected that ion migration causes the degradation;^[35] however, the AgI impurity and its effects on the device degradation were not investigated.

The device performance degradation of the Ag_3BiI_6 device was suspected to be due to 1) the presence of a high amount of residual AgI near the surface and/or 2) due to the voids at the interface of TiO_2 . This further indicates that a void-free layer might help in enhancing stability. Therefore, to investigate this, we obtained void-free Ag_3BiI_6 thin film by depositing it without antisolvent and compared it with the Ag_3BiI_6 device processed with antisolvent dripping. The XRD pattern of Ag_3BiI_6 with and without voids, as shown in Figure 2a and Figure S2c, Supporting Information, showed an insignificant difference.^[19,20] However, the XRD pattern of Ag_3BiI_6 thin film processed with antisolvent (Figure 2a) showed higher peak intensity compared with without antisolvent case evidencing improved crystallinity. Residual AgI was also observed in the XRD pattern of the without antisolvent-processed Ag_3BiI_6 thin film, as shown in Figure S2c, Supporting Information. The ratio of XRD peak intensities of AgI and Ag_3BiI_6 with respect to highest peak intensity oriented along (003) crystal plane, as shown in Figure S9, Supporting Information, clearly indicates the insignificant difference in the amount of residual AgI in without and with antisolvent-processed Ag_3BiI_6 thin films. The nonexistence of Ag_3BiI_6 in a pure single phase at room temperature can be the reason for the residual AgI content.^[19] The unreacted or residual AgI might also lead to unreacted/residual BiI_3 ; however, the residual BiI_3 peaks were not detected in the XRD pattern most probably due to the overlapping of some of the BiI_3 and Ag_3BiI_6 XRD peaks, as shown in Figure S10, Supporting Information. In contrast to the antisolvent-based Ag_3BiI_6 case, without antisolvent-based Ag_3BiI_6 device showed bright dots primarily near the

mesoporous TiO_2 layer (Figure 2b) with no voids. Another cross-sectional SEM image showing bright dots near the TiO_2 interface and void-free layer is shown in Figure S11, Supporting Information. The difference in the location of bright dots can further be corroborated from top surface SEM images. Figure 2c shows a small amount of bright dots on the surface of Ag_3BiI_6 grains that was processed without the antisolvent dripping step. On the contrary, these dots were observed in a higher amount near the grain boundaries for the antisolvent case, as shown in Figure 2d. This further suggests the presence of a higher amount of residual AgI on the surface of Ag_3BiI_6 grains and at the $\text{Ag}_3\text{BiI}_6/\text{P3HT}/\text{Au}$ interface. In case of without antisolvent, Ag_3BiI_6 thin film showed circular morphology whereas slightly flat morphology was observed in the case of anti-solvent, as shown in Figure 2c,d, respectively. The difference in the morphology compared with previous reports^[20,32] is mostly due to the choice of solvent and thin-film processing conditions. True non-contact atomic force microscope (AFM) measurements (Figure S12b, Supporting Information) substantiated low root mean square (RMS) roughness of 15 nm and improved surface uniformity for Ag_3BiI_6 film processed with antisolvent dripping in comparison with without antisolvent case (Figure S12a, Supporting Information) which showed RMS roughness of 70 nm and is in line with top surface SEM morphology.

Photophysical properties of Ag_3BiI_6 films processed without and with antisolvent were investigated by steady-state photoluminescence (PL). This investigation helps to gain insights into the effect of antisolvent dripping and residual AgI on the charge carrier recombination in Ag_3BiI_6 film. A broad PL peak was observed, as shown in Figure S13a, Supporting Information, which is consistent with the previous report.^[19] Moreover, PL analysis showed a higher peak intensity for antisolvent-based Ag_3BiI_6 film compared with without antisolvent one. A blueshift in the PL peak (Figure S13b, Supporting Information) was correspondingly observed for Ag_3BiI_6 film processed with antisolvent. The exact reason for the enhanced PL peak intensity and blueshift is not known at the moment, but it might be due to low trap/defect sites and recombination centers^[36,37] in the bulk of Ag_3BiI_6 and/or could also

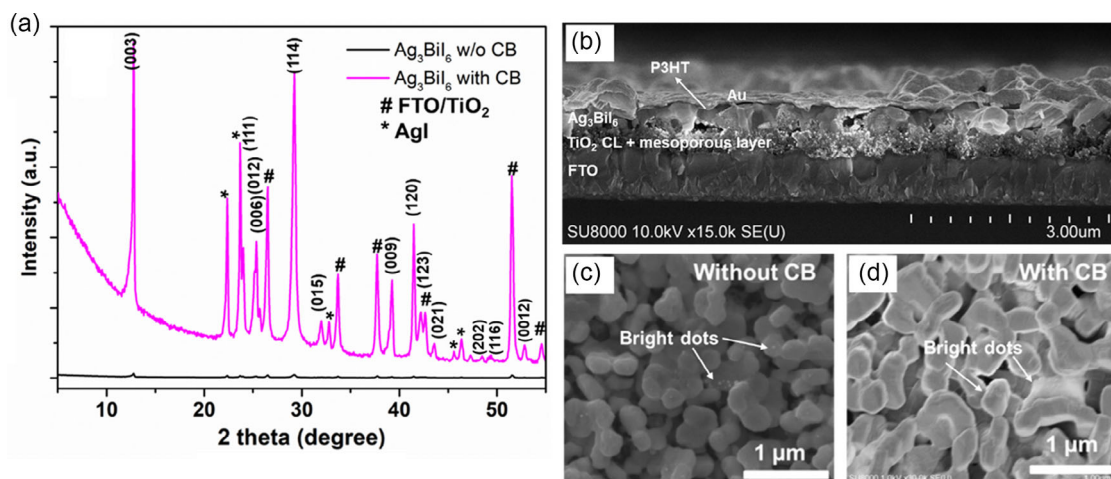


Figure 2. a) XRD pattern of Ag_3BiI_6 thin film processed with and without antisolvent; the peaks were indexed according to the data from Oldag et al.,^[27] b) cross-sectional SEM image of Ag_3BiI_6 solar cell processed without antisolvent method; top-view SEM images of Ag_3BiI_6 thin film c) without and d) with antisolvent dripping.

be within the experimental error mostly because of the existence of impure phase or multiphase features. In addition to this, the PL showed a small additional peak at around ≈ 735 nm which can be ascribed to the Ag_3BiI_6 impure phase (presence of residual AgI) and/or multiphase features.^[19,20,32]

Photovoltaic characteristics were studied to elucidate the effect of a void-free layer on efficiency and stability. From the J - V characteristic curves (Figure 3a, Supporting Information) of the best performing device and the box plots (Figure S14, Supporting Information), it is evident that Ag_3BiI_6 devices processed without antisolvent dripping showed better photovoltaic performance (best device showed PCE of 2.3%) in comparison with antisolvent-based Ag_3BiI_6 devices (best device showed PCE of 1.8%). The obtained efficiency (for without antisolvent case) is among the best in the same category of Ag_3BiI_6 solar cells using dopant-free P3HT as HTL.^[20] The antisolvent-processed device showed large hysteresis in the device J - V curve compared with without antisolvent one, as shown in Figure S15a, Supporting Information. The incident photon-to-current efficiency (IPCE) spectra of the best performing device and the photovoltaic device parameters are shown and tabulated in Figure S15b and Table S2, Supporting Information, respectively. Despite showing enhanced PL peak intensity, the presence of voids and a nonuniform interface in antisolvent-based Ag_3BiI_6 devices attributes to low efficiency. On exposure to ambient atmosphere (humidity = 30–50%), without antisolvent-based Ag_3BiI_6 device degraded slowly (after 15 weeks) as compared with with antisolvent one (after 1 week), as shown in Figure 3b. The performance degradation was additionally accompanied by a visual change in the color of the Au metal electrode, as shown in Figure 3c, evidencing its degradation. It is important to note that for without antisolvent

case, the visual color of Au changed after several weeks whereas in the case of antisolvent-based Ag_3BiI_6 device the Au decomposed in 2 weeks, and prolonged exposure to ambient atmosphere resulted in a complete change in the color of the substrate (Figure 3c) indicating complete device failure.

To understand the Ag_3BiI_6 device degradation in the presence of other dopant-free HTL, we used a dopant-free conjugated copolymer poly[(dithieno[3,2-*b*:2',3'-*d*]silolethieno[3,4-*c*]pyrrole-4,6-dione)-random-(2,2'-bithiophenethieno[3,4-*c*]pyrrole-4,6-dione)] (poly(DTSTPD-*r*-BThTPD)) HTL. The structure of the (poly(DTSTPD-*r*-BThTPD)) HTL is shown in Figure S16a, Supporting Information. This HTL was previously synthesized and used by our group in all-inorganic-based lead perovskite solar cells showing high V_{OC} .^[7,38] When the same HTL was used, the Ag_3BiI_6 device showed slight enhancement in the V_{OC} compared with the P3HT HTL (Figure S16b, Supporting Information). However, the Au deposited on poly(DTSTPD-*r*-BThTPD) HTL decomposed in 2 weeks similar to that of the P3HT case (Figure S16c, Supporting Information), clearly indicating that the Ag_3BiI_6 device degradation is independent of the HTLs used. To understand the sensitivity of Ag_3BiI_6 thin film under ambient humidity conditions, we intentionally stored antisolvent-processed Ag_3BiI_6 film in ambient conditions for 2 weeks followed by deposition of P3HT and Au and compared their structural, morphological, and photovoltaic performance with the ones that were freshly prepared. As can be seen in Figure S17 and Figure S18, Supporting Information, the UV-vis absorption spectra, XRD pattern, surface morphology, and the performance of the device made of Ag_3BiI_6 films which were intentionally stored for 2 weeks showed insignificant difference compared with that of freshly prepared Ag_3BiI_6 thin-film

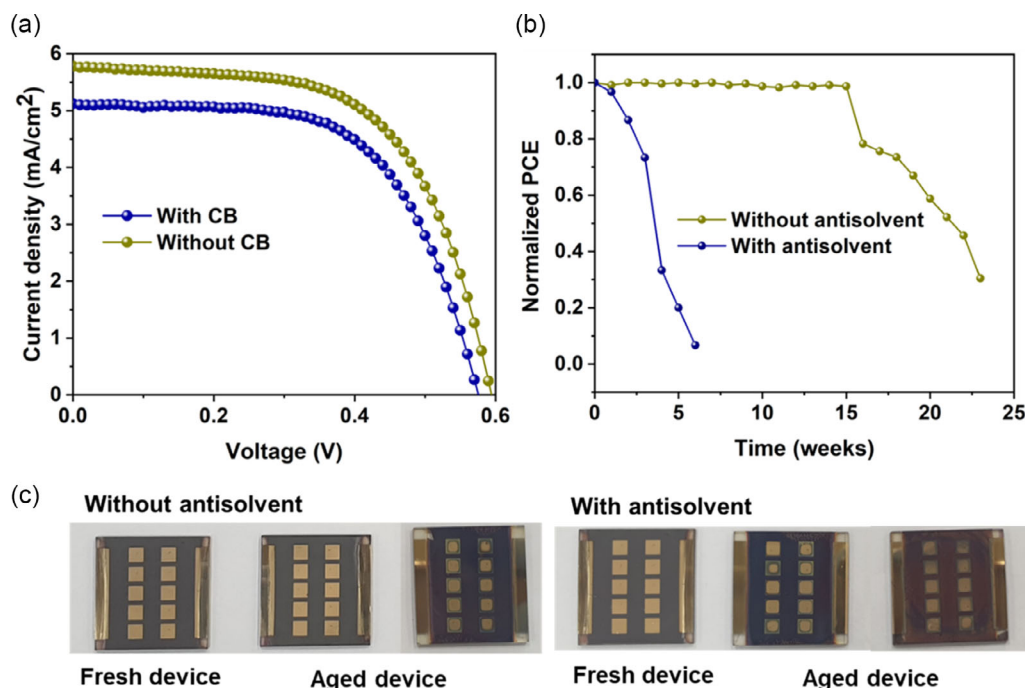


Figure 3. Performance and stability of Ag_3BiI_6 solar cells fabricated with and without the antisolvent method: a) J - V curves of best performing solar cells of thin films with and without antisolvent; b) stability of the PCE over several weeks; and c) photographs of fresh and aged Ag_3BiI_6 solar cell devices showing slow and fast degradation for without and with antisolvent case.

and devices. The UV–vis spectrum of fresh Ag_3BiI_6 thin film is shown in Figure S23, Supporting Information, and details will be discussed later. Interestingly, the performance of a device made of aged Ag_3BiI_6 thin film degraded only after depositing the P3HT and Au electrode and the degradation trend was similar to that of the device obtained from freshly prepared Ag_3BiI_6 device, as shown in Figure S18b, Supporting Information. This degradation can be possibly related to the internal electric field-driven migration and diffusion of ions toward the Au electrode which is corroborated by large hysteresis in the device J – V curve (Figure S15a, Supporting Information) for the antisolvent-based device, suggesting a high amount of ion migration and faster degradation compared with without antisolvent case. According to a previous report, part of silver which is localized in the Ag_3BiI_6 crystal structure varies with temperature and moves within the crystal structure.^[27] From this, it can be envisaged that the residual AgI that is observed in Ag_3BiI_6 thin film causes migration through thin P3HT HTL to corrode the Au electrode and degrade the performance as both Ag^+ and I^- are highly mobile due to low activation energy. Moreover, fast degradation in the antisolvent case indicates that the voids at the $\text{TiO}_2/\text{Ag}_3\text{BiI}_6$ interface and accumulation of residual AgI on the surface can cause migration and diffusion of ions at a faster rate. It is important to note that devices were stored in an ambient atmosphere in the presence of light and to verify the migration of ions in the presence of light, the antisolvent-processed Ag_3BiI_6 device was exposed to 1 sun (100 mW cm^{-2}) continuous illumination held at maximum power point tracking (MPPT). As can be seen from Figure S19, Supporting Information, the Ag_3BiI_6 device containing voids and Ag-rich phase near the $\text{Ag}_3\text{BiI}_6/\text{P3HT}/\text{Au}$ interface showed slow but linear degradation; however, it maintained PCE up to $\approx 1.5\%$ (initial efficiency = 1.8%) after 5000 s, indicating that light illumination (in addition to ambient atmosphere) might cause ion migration and performance degradation. The decomposition of AgI via photochemical reaction^[39] hints toward the linear and slow degradation of the performance under continuous light illumination.

To confirm the migration of Ag^+ and I^- ions and their role in performance deterioration, X-ray photoelectron spectroscopy (XPS) was performed on the aged device showing both yellow (nondegraded region) and green (degraded region) areas of Au, and the results are shown in Figure 4. The XPS peaks on the yellow part of the Au (Figure 4a inset) appeared at 84.2 and 87.8 eV belonging to the $4f_{7/2}$ and $4f_{5/2}$ orbitals, respectively, as shown in Figure 4a. These values belong to the metallic form of Au which appears at 84 and 88 eV.^[40,41] These 4f XPS peaks, on the degraded part of Au (Figure 4b inset), showed a shift from metallic (84.2 and 87.8 eV) to higher binding energy (84.9 and 88.6 eV) evidencing oxidation of Au^0 to Au^{+1} .^[42] Moreover, a small peak corresponding to Au^{+3} was also observed at around 86 eV, as shown in Figure 4b.^[41] In addition to this, a relatively large amount of iodine ($3d_{5/2}$ peak) was detected (Figure 4c,d) on the surface of the Au. The migration of residual AgI to the Au electrode top surface can be the source of iodine because Ag $3d$ peak was detected on the surface of Au, as shown in Figure 4e,f. The presence of Ag^+ and I^- corroborates the cross-sectional SEM image (Figure S6, Supporting Information) showing bright dots on the surface of the Au. We observed Ag $3d$ peak at 368.17 eV on the yellow area (nondegraded region) and at 368.3 eV on the

green area (degraded region) assigning to Ag^+ (AgI) and Ag^0 , respectively.^[43] This peak shift from lower binding energy to higher binding energy indicates the reduction of AgI to Ag metallic. Another image showing a slight shift in the peak position of Ag is shown in Figure S20, Supporting Information. In addition to this, it was surprising to observe the presence of bismuth (Bi^{3+}) on the surface of the Au top electrode. Although Bi^{3+} has a large ionic radius and high ion migration energy barrier (3.363 eV), we suspect that the presence of voids might have facilitated the migration of Bi^{3+} . In the yellow area of Au, high intense and low intense Bi 4f peaks^[40] (Figure 4g) appeared corresponding to Bi^{3+} and Bi^0 , respectively.^[44] According to previous reports, BiI_3 possesses a lot of interstitial defects, where bismuth is not bonded to iodine atoms.^[45,46] This might be the reason for the appearance of the Bi^0 peak in the XPS spectra. There could also be a possibility arising from impurities or admixtures leading to the presence of metallic bismuth. Interestingly, the intensity of the Bi^0 metallic peak at 157 eV becomes intense in the green region (degraded part) of the Au (Figure 4h), indicating reduction of the higher amount of Bi^{3+} to metallic Bi^0 and removal of iodide. Chemical shifts of Au cannot be clearly explained by the physisorption of AgI or BiI_3 or I_2 on the surface of electrodes. Instead, the oxidation of Au^0 to Au^{+1} and Au^{+3} , presence of iodine, and reduction of Ag^+ to Ag^0 and Bi^{3+} to Bi^0 indicate that Au has reacted with iodine leading to degradation of the cell.

To understand the triple-ion migration and phase separation of BiI_3 and AgI, we have performed first-principles electronic structure calculations within the density functional theory (DFT) framework to provide additional insight from the perspective of electronic and optical properties of the material (detailed DFT simulations can be found in Explanation E2, Supporting Information). From the total density of states (DOS) (Figure S22, Supporting Information), calculated by hybrid functional (HSE06) considering the spin–orbit coupling of the heavy metal Bi, we observed a bandgap of 1.8 eV, which agrees with our experimental results (UV–vis spectra of Ag_3BiI_6 thin film and its corresponding Tauc plot are shown in Figure S23, Supporting Information). With the help of our total energy calculations based on the DFT formalism, we determined the decomposition enthalpy of the possible degradation pathway of Ag_3BiI_6 . The decomposition enthalpy is calculated specifically for the degradation pathway: $\text{Ag}_3\text{BiI}_6 \xrightarrow{\Delta H} 3\text{AgI} + \text{BiI}_3$, where the minimum energy configuration of the individual bulk system has been achieved through complete ionic relaxation. The corresponding decomposition enthalpy (ΔH) was found to be -0.053 eV per formula unit, where the negative sign signifies the favorable degradation to occur as an exothermic reaction. This resembles well with the experimental result, where the degradation of Ag_3BiI_6 to AgI and BiI_3 is observed.

Based on the experimental and theoretical results, a possible Ag_3BiI_6 device degradation mechanism is proposed as shown in Figure 5. From the theoretical studies, we observed low decomposition energy which results in the degradation of Ag_3BiI_6 material to AgI and BiI_3 . This corroborates with the XRD pattern where we observed residual AgI content within the Ag_3BiI_6 thin film. Several factors can account for the migration of AgI and BiI_3 and corrosion of Au which includes the decomposition of AgI

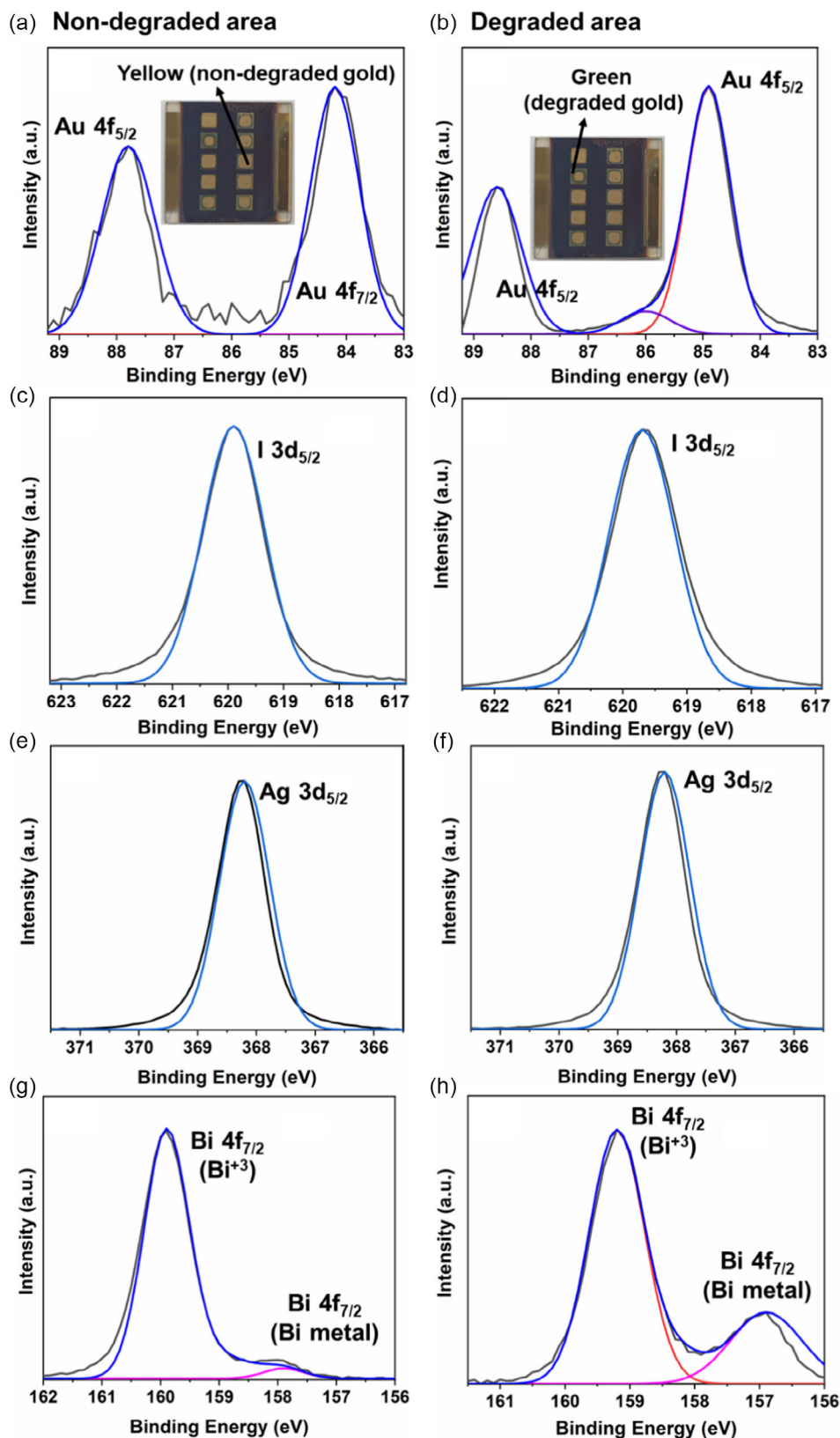


Figure 4. XPS core-level spectra of a–b) gold 4f; c–d) iodine 3d; e–f) silver 3d; and g–h) bismuth 4f of nondegraded electrode area and degraded electrode area, respectively.

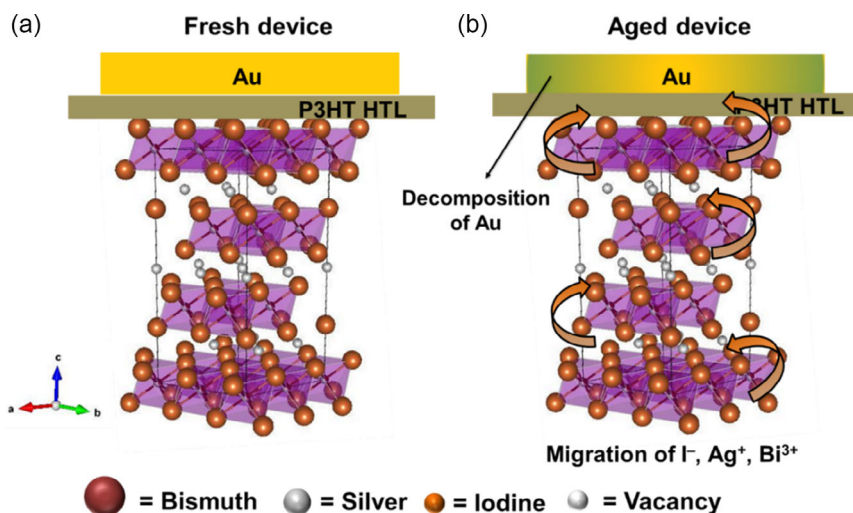


Figure 5. Schematic illustration of the proposed mechanism of a) fresh and b) aged Ag_3BiI_6 device showing the degradation in aged device under ambient atmosphere (RH = 30–50%).

due to photochemical reaction^[39] and the reaction of iodide/iodine with Au. When exposed to continuous light illumination, Ag_3BiI_6 device showed linear and slow degradation (Figure S19, Supporting Information) hinting toward the photochemical decomposition of residual AgI.^[39] The similar and low activation energy of Ag^+ and I^- suggests fast migration of these ions. In the case of bismuth, although BiI_3 has a high migration barrier, lesser known underpotential deposition (UPD) reaction has been reported previously, showing adsorption of BiI_3 on the surface of the Au and reduction of Bi^{3+} to Bi^0 and reaction of Au with iodide/iodine.^[47] The UPD adsorption reaction was also observed in Ag^+ on the surface of Au.^[48] This phenomenon was also observed in lead perovskite solar cells in which Pb^{2+} in MAPbI_3 reduced to Pb^0 when interfaced with Au.^[49] We suspect that UPD reaction might occur at the $\text{Ag}_3\text{BiI}_6/\text{P3HT}$ (or poly(DTSTPD-*r*-BThTPD))/Au interface because of a very thin layer of HTL leading to reduction of Bi^{3+} to Bi^0 and Ag^+ to Ag^0 and corrosion of Au electrodes. However, a detailed investigation is required to validate this and is in progress. In addition, the effect of internal electric field leading to migration of Ag^+ , Bi^{3+} , and I^- species and corrosion of Au cannot be neglected. During the Ag_3BiI_6 crystallization, intrinsic point defects can potentially form, including interstitial defects, elemental vacancy, and so on.^[50] In addition to these defects, voids that are observed in antisolvent-processed Ag_3BiI_6 thin film (Figure 1e) become the dominant defects that facilitate the migration of ions. The previous report suggests the presence of vacancies in the Ag_3BiI_6 crystal structure.^[27] Considering the vacancies, defects, interstitial sites, and voids, in addition to interstitial defects/admixtures that are present within BiI_3 ,^[45] it is reasonable to propose vacancy-mediated ion migration in Ag_3BiI_6 thin film. The migration of Ag^+ , Bi^{3+} , I^- ions near the interface with the P3HT (and poly(DTSTPD-*r*-BThTPD)) HTL promotes the diffusion of bulk elements toward the surface mainly due to the concentration gradient to achieve thermodynamic equilibrium. This further leads to the continuous loss of Bi^{3+} , Ag^+ , and I^- ions from the bulk. The oxidation of Au to Au^{+1} , presence of iodine,

and reduction of Ag^+ and Bi^{3+} (Figure 4) on the surface of Au indicate the migration and diffusion of ions through thin P3HT (and poly(DTSTPD-*r*-BThTPD)) layers and the reaction of Au with iodine to possibly form gold iodide (AuI), thereby degrading the cell. It is interesting to observe that two oppositely charged ions (i.e., Bi^{3+} and I^- or Ag^+ and I^-) accumulate at the same interface. We speculate that the reactivity of the Au electrode with volatile halide ions might partially contribute to this unusual and unique phenomenon. As we used a thin layer of HTL, we suspect that this triple-ion migration to the electrode interface and degradation of Au can be protected by using a thick HTL. To verify this, we initially used thick P3HT layer by changing the spin-coating condition. To increase the thickness, the concentration of P3HT was fixed to 15 mg mL^{-1} and the spinning condition was altered. However, the PCE reduced (PCE statistics is shown in Figure S24, Supporting Information) with an increase in the thickness of P3HT HTL mostly ascribing to increase in the resistance at the $\text{Ag}_3\text{BiI}_6/\text{P3HT}$ interface. Therefore, we fabricated Ag_3BiI_6 devices with 2,2',7,7'-Tetrakis[*N,N*-di(4-methoxyphenyl)amino]-9,9'-spirobifluorene (spiro-OMeTAD) as HTL. We have used spiro-OMeTAD with ethanol (EtOH) and lithium bis(trifluoromethanesulfonyl)imide (Li-TFSI) dopants^[51] because the combination of widely used Li-TFSI and 4-*tert*-butylpyridine (TBP) dopants rapidly corrodes the Ag_3BiI_6 layer. The optical microscopic images showing corrosion of the Ag_3BiI_6 layer with HTL (without and with Li-TFSI and TBP dopants) are shown in Figure S25, Supporting Information. After exposing the spiro-OMeTAD HTL-based device to the ambient atmosphere, no visible change in the color of the Au electrode was observed and the device showed stable efficiency, as shown in Figure S26b, Supporting Information, suggesting the suppression of ion migration. The *J*-*V* curve of the Ag_3BiI_6 device using spiro-OMeTAD is shown in Figure S26a, Supporting Information. Based on our present results, we presume that suppressing residual AgI content might help to avoid Ag_3BiI_6 material and device degradation. Phase pure Ag_3BiI_6 without residual AgI might be obtained by exploring suitable solvents and/or

additives. Efforts to replace the Au metal electrode with a more stable and inert electrode can also be a significant step in enhancing the stability. Despite the antagonistic influence on photovoltaic device stability, the migration of ions in Ag_3BiI_6 can allow its extensive application in photodetectors^[52] (to facilitate fast response) and in resistive-switching memory devices.^[53]

3. Conclusion

In conclusion, this work reported efficient solar cells based on AgBi_2I_7 , Ag_2BiI_5 , and Ag_3BiI_6 light absorbers. The long-term stability of devices under ambient humidity atmosphere reveals that Ag_3BiI_6 adopts unique triple-ion migration where Ag^+ , Bi^{3+} , and I^- ions migrate and diffuse through HTL contrasting the case of Ag_2BiI_5 and AgBi_2I_7 . The theoretical study suggests that low decomposition enthalpy favors the decomposition of Ag_3BiI_6 to AgI and BiI_3 causing migration and diffusion of ions. This migration is more pronounced in antisolvent-processed Ag_3BiI_6 thin film-based devices as it showed faster degradation in the device performance compared with without antisolvent one and was relieved by using a thick HTL in solar cells. The unusual triple-ion migration behavior in Ag_3BiI_6 accentuates the importance of not only understanding and improving the Ag_3BiI_6 material for better solar cell design but also stimulating the use of this unique behavior in other optoelectronics such as photodetector and switching memory devices.

Supporting Information

Supporting Information is available from the Wiley Online Library or from the author.

Acknowledgements

A.K. and F.Ü. contributed equally to this work. The present research has been supported by the Japanese Society for Promotion of Science (JSPS) with Grant-in-Aid for Scientific Research S as well as for International Fellowships for Research Program. A.K. thanks funding support from the Japan Society for Promotion of Sciences (JSPS) postdoctoral (PD) fellowship. F.Ü. and S.M. gratefully acknowledge the University of Cologne (Excellence Program "Quantum Matter and Materials") and the German Science Foundation (DFG) for the funding provided in the framework of the Priority Program SPP2196. The authors thank DAAD for a bilateral mobility grant supporting the exchange visit of researchers between the University of Cologne, Germany, and the RMIT University, Melbourne, Australia (Project-ID 57388639). The authors acknowledge Hanming Liu, Daniele Cuzzupe, and Khan Lê for PL measurements. The authors acknowledge Mitsubishi Chemical Cooperation for their support in providing poly(DTSTPD-*r*-BThTPD) hole transport layer. The authors acknowledge Professor H. Segawa for providing access to research facilities at Research Center for Advanced Science and Technology (RCAST), The University of Tokyo.

Conflict of Interest

The authors declare no conflict of interest.

Data Availability Statement

Research data are not shared.

Keywords

degradation, gold electrodes, ion migration, lead-free solar cells, silver bismuth iodide, solar cells, stability

Received: January 29, 2021
Revised: June 7, 2021
Published online: July 8, 2021

- [1] A. Kojima, K. Teshima, Y. Shirai, T. Miyasaka, *J. Am. Chem. Soc.* **2009**, 131, 6050.
- [2] A. K. Jena, A. Kulkarni, T. Miyasaka, *Chem. Rev.* **2019**, 119, 3036.
- [3] NREL, *Best Research-Cell Efficiency Chart* **2021**, <https://www.nrel.gov/pv/cell-efficiency.html> (accessed: May 2021).
- [4] T. Miyasaka, A. Kulkarni, G. M. Kim, S. Öz, A. K. Jena, *Adv. Energy Mater.* **2020**, 10, 1902500.
- [5] M. H. Futscher, J. M. Lee, L. McGovern, L. A. Muscarella, T. Wang, M. I. Haider, A. Fakharuddin, L. Schmidt-Mende, B. Ehrler, *Mater. Horizons* **2019**, 6, 1497.
- [6] N. Liu, C. Yam, *Phys. Chem. Chem. Phys.* **2018**, 20, 6800.
- [7] S. Öz, A. K. Jena, A. Kulkarni, K. Mouri, T. Yokoyama, I. Takei, F. Ünlü, S. Mathur, T. Miyasaka, *ACS Energy Lett.* **2020**, 5, 1292.
- [8] N. Pant, A. Kulkarni, M. Yanagida, Y. Shirai, T. Miyasaka, K. Miyano, *Adv. Mater. Interfaces* **2020**, 7, 1901748.
- [9] A. Babayigit, A. Ethirajan, M. Muller, B. Conings, *Nat. Mater.* **2016**, 15, 247.
- [10] S. Gu, R. Lin, Q. Han, Y. Gao, H. Tan, J. Zhu, *Adv. Mater.* **2020**, 32, 1907392.
- [11] Z. Jin, Z. Zhang, J. Xiu, H. Song, T. Gatti, Z. He, *J. Mater. Chem. A* **2020**, 8, 16166.
- [12] B. Ghosh, S. Chakraborty, H. Wei, C. Guet, S. Li, S. Mhaisalkar, N. Mathews, *J. Phys. Chem. C* **2017**, 121, 17062.
- [13] B. Ghosh, B. Wu, H. K. Mulmudi, C. Guet, K. Weber, T. C. Sum, S. Mhaisalkar, N. Mathews, *ACS Appl. Mater. Interfaces* **2018**, 10, 35000.
- [14] A. Kulkarni, T. Singh, M. Ikegami, T. Miyasaka, *RSC Adv.* **2017**, 7, 9456.
- [15] B. W. Park, B. Philippe, X. Zhang, H. Rensmo, G. Boschloo, E. M. J. Johansson, *Adv. Mater.* **2015**, 27, 6806.
- [16] Y. Kim, Z. Yang, A. Jain, O. Voznyy, G. H. Kim, M. Liu, L. N. Quan, F. P. García de Arquer, R. Comin, J. Z. Fan, E. H. Sargent, *Angew. Chem. Int. Ed.* **2016**, 55, 9586.
- [17] A. Kulkarni, A. K. Jena, M. Ikegami, T. Miyasaka, *Chem. Commun.* **2019**, 55, 4031.
- [18] H. Zhu, M. Pan, M. B. Johansson, E. M. J. Johansson, *ChemSusChem* **2017**, 10, 2592.
- [19] I. Turkevych, S. Kazaoui, E. Ito, T. Urano, K. Yamada, H. Tomiyasu, H. Yamagishi, M. Kondo, S. Aramaki, *ChemSusChem* **2017**, 10, 3754.
- [20] N. Pai, J. Lu, T. R. Gengenbach, A. Seeber, A. S. R. Chesman, L. Jiang, D. C. Senevirathna, P. C. Andrews, U. Bach, Y.-B. Cheng, A. N. Simonov, *Adv. Energy Mater.* **2018**, 9, 1803396.
- [21] Y. Seo, S. R. Ha, S. Yoon, S. M. Jeong, H. Choi, D.-W. Kang, *J. Power Sources* **2020**, 453, 227903.
- [22] A. K. Baranwal, H. Masutani, H. Sugita, H. Kanda, S. Kanaya, N. Shibayama, Y. Sanehira, M. Ikegami, Y. Numata, K. Yamada, T. Miyasaka, T. Umeyama, H. Imahori, S. Ito, *Nano Conver.* **2017**, 4, 26.

- [23] H.-W. Chen, N. Sakai, M. Ikegami, T. Miyasaka, *J. Phys. Chem. Lett.* **2015**, 6, 164.
- [24] H. J. Snaith, A. Abate, J. M. Ball, G. E. Eperon, T. Leijtens, N. K. Noel, S. D. Stranks, J. T. W. Wang, K. Wojciechowski, W. Zhang, *J. Phys. Chem. Lett.* **2014**, 5, 1511.
- [25] A. K. Jena, A. Kulkarni, M. Ikegami, T. Miyasaka, *J. Power Sources* **2016**, 309, 1.
- [26] Y. Yuan, Q. Wang, J. Huang, in *Organic-Inorganic Halide Perovskite Photovoltaics: From Fundamentals to Device Architectures* (Eds.: N. G. Park, M. Grätzel, T. Miyasaka), Springer, Cham **2016**, pp. 137–162.
- [27] T. Oldag, T. Aussieker, H. L. Keller, C. Preitschaft, A. Pfizner, *Z. Anorg. Allg. Chem.* **2005**, 631, 677.
- [28] J. L. Minns, P. Zajdel, D. Chernyshov, W. van Beek, M. A. Green, *Nat. Commun.* **2017**, 8, 15152.
- [29] C. Besleaga, L. E. Abramiuc, V. Stancu, A. G. Tomulescu, M. Sima, L. Trinca, N. Plugaru, L. Pintilie, G. A. Nemnes, M. Iliescu, H. G. Svavarsson, A. Manolescu, I. Pintilie, *J. Phys. Chem. Lett.* **2016**, 7, 5168.
- [30] A. Koedtrud, M. Goto, M. Amano Patino, Z. Tan, H. Guo, T. Nakamura, T. Handa, W. T. Chen, Y. C. Chuang, H. S. Sheu, T. Saito, D. Kan, Y. Kanemitsu, A. Wakamiya, Y. Shimakawa, *J. Mater. Chem. A* **2019**, 7, 5583.
- [31] L. F. Mashadiev, Z. S. Aliev, A. V. Shevelkov, M. B. Babanly, *J. Alloys Compd.* **2013**, 551, 512.
- [32] B. Ghosh, B. Wu, X. Guo, P. C. Harikesh, R. A. John, T. Baikie, Arramel, A. T. S. Wee, C. Guet, T. C. Sum, S. Mhaisalkar, N. Mathews, *Adv. Energy Mater.* **2018**, 8, 1802051.
- [33] Y. Bekenstein, J. C. Dahl, J. Huang, W. T. Osowiecki, J. K. Swabeck, E. M. Chan, P. Yang, A. P. Alivisatos, *Nano Lett.* **2018**, 18, 3502.
- [34] S. Svanström, T. J. Jacobsson, G. Boschloo, E. M. J. Johansson, H. Rensmo, U. B. Cappel, *ACS Appl. Mater. Interfaces* **2020**, 12, 7212.
- [35] A. Crovetto, A. Hajjafarassar, O. Hansen, B. Seger, I. Chorkendorff, P. C. K. Vesborg, *Chem. Mater.* **2020**, 32, 3385.
- [36] N. Pant, A. Kulkarni, M. Yanagida, Y. Shirai, T. Miyasaka, K. Miyano, *ACS Appl. Energy Mater.* **2020**, 3, 6215.
- [37] T. Kirchartz, J. A. Márquez, M. Stollerfoht, T. Unold, *Adv. Energy Mater.* **2020**, 10, 1904134.
- [38] Z. Guo, A. K. Jena, I. Takei, G. M. Kim, M. A. Kamarudin, Y. Sanehira, A. Ishii, Y. Numata, S. Hayase, T. Miyasaka, *J. Am. Chem. Soc.* **2020**, 142, 9725.
- [39] E. J. Hartung, *J. Chem. Soc.* **1926**, 129, 1349.
- [40] J. F. Moulder, J. Chastain, *Handbook of X-Ray Photoelectron Spectroscopy: A Reference Book of Standard Spectra for Identification and Interpretation of XPS Data*, Physical Electronics Division, Perkin-Elmer Corporation, Eden Prairie, MN **1992**.
- [41] K. Kwon, B. L. Suh, K. Park, J. Kim, H.-T. Jung, *Sci. Rep.* **2019**, 9, 3885.
- [42] M. P. Casaletto, A. Longo, A. Martorana, A. Prestianni, A. M. Venezia, *Surf. Interface Anal.* **2006**, 38, 215.
- [43] Y. Kato, L. K. Ono, M. V. Lee, S. Wang, S. R. Raga, Y. Qi, *Adv. Mater. Interfaces* **2015**, 2, 1500195.
- [44] W. E. Morgan, W. J. Stec, J. R. Van Wazer, *Inorg. Chem.* **1973**, 12, 953.
- [45] A. Kulkarni, T. Singh, A. K. Jena, P. Pinpithak, M. Ikegami, T. Miyasaka, *ACS Appl. Mater. Interfaces* **2018**, 10, 9547.
- [46] W. Czaja, G. Harbeke, L. Krausbauer, E. Meier, B. J. Curtis, H. Brunner, E. Tosatti, *Solid State Commun.* **1973**, 13, 1445.
- [47] Y.-L. Du, C.-M. Wang, *Chinese J. Chem.* **2002**, 20, 596.
- [48] E. Herrero, L. J. Buller, H. D. Abruña, *Chem. Rev.* **2001**, 101, 1897.
- [49] R. A. Kerner, P. Schulz, J. A. Christians, S. P. Dunfield, G. Teeter, J. J. Berry, B. P. Rand, *APL Mater.* **2019**, 7, 041103.
- [50] L. Liang, P. Gao, *Adv. Sci.* **2018**, 5, 1700331.
- [51] Z. Hu, Z. Wang, G. Kapil, T. Ma, S. Iikubo, T. Minemoto, K. Yoshino, T. Toyoda, Q. Shen, S. Hayase, *ChemSusChem* **2018**, 11, 2930.
- [52] H. Wang, M. Zhou, H. Luo, *ACS Omega* **2018**, 3, 1445.
- [53] X. Guan, W. Hu, M. A. Haque, N. Wei, Z. Liu, A. Chen, T. Wu, *Adv. Funct. Mater.* **2018**, 28, 1704665.